Reactive Quenching Of Od A (2)Σ(+) By H-2: Translational Energy Distributions For H- And D-Atom Product Channels

J. H. Lehman

Jesse Lyle Bertrand , '11

Thomas Alex Stephenson
Swarthmore College, tstephe1@swarthmore.edu

M. I. Lester

Recommended Citation

J. H. Lehman; Jesse Lyle Bertrand , '11; Thomas Alex Stephenson; and M. I. Lester. (2011). "Reactive Quenching Of Od A (2)Σ(+) By H-2: Translational Energy Distributions For H- And D-Atom Product Channels". *Journal Of Chemical Physics*. Volume 135, Issue 14. DOI: 10.1063/1.3644763
https://works.swarthmore.edu/fac-chemistry/13

Reactive quenching of OD A 2+ by H2: Translational energy distributions for H- and D-atom product channels

Julia H. Lehman, Jesse L. Bertrand, Thomas A. Stephenson, and Marsha I. Lester

Reactive quenching of OD A $^2\Sigma^+$ by H$_2$: Translational energy distributions for H- and D-atom product channels

Julia H. Lehman,[1] Jesse L. Bertrand,[2] Thomas A. Stephenson,[2] and Marsha I. Lester[1,a)]

[1]*Department of Chemistry, University of Pennsylvania, Philadelphia, Pennsylvania 19104-6323, USA*
[2]*Department of Chemistry and Biochemistry, Swarthmore College, Swarthmore, Pennsylvania 19081, USA*

The H- and D-atom products from collisional quenching of OD A $^2\Sigma^+$ by H$_2$ are characterized through Doppler spectroscopy using two-photon (2 ^{2}S $\leftarrow\leftarrow$ 1 ^{2}S) laser-induced fluorescence. Partial deuteration enables separation of the channel forming H + HOD products, which accounts for 75% of reactive quenching events, from the D + H$_2$O product channel. The Doppler profiles, along with those reported previously for other isotopic variants, are transformed into product translational energy distributions using a robust fitting procedure based on discrete velocity basis functions. The product translational energy distribution for the H-atom channel is strongly peaked at low energy (below 0.5 eV) with a long tail extending to the energetic limit. By contrast, the D-atom channel exhibits a small peak at low translational energy with a distinctive secondary peak at higher translational energy (approximately 1.8 eV) before falling off to higher energy. In both cases, most of the available energy flows into internal excitation of the water products. Similar distributions are obtained upon reanalysis of D- and H-atom Doppler profiles, respectively, from reactive quenching of OH A $^2\Sigma^+$ by D$_2$. The sum of the translational energy distributions for H- and D-atom channels is remarkably similar to that obtained for OH A $^2\Sigma^+$ + H$_2$, where the two channels cannot be distinguished from one another. The product translational energy distributions from reactive quenching are compared with those obtained from a previous experiment performed at higher collision energy, quasiclassical trajectory calculations of the post-quenching dynamics, and a statistical model. © *2011 American Institute of Physics*. [doi:10.1063/1.3644763]

I. INTRODUCTION

The hydroxyl radical is an important species in atmospheric and combustion environments, where it is often detected using laser-induced fluorescence (LIF) on the OH A $^2\Sigma^+$ – X $^2\Pi$ band system.[1] However, collisions with molecular partners abundant in these environments are known to efficiently remove OH from the excited A $^2\Sigma^+$ state, resulting in reduced fluorescence lifetimes and quantum yields. The rate of this collisional quenching process has been studied for a variety of molecular partners over a wide range of temperatures and initial OH A $^2\Sigma^+$ rotational states.[2–7] In general, the rates were found to decrease with increasing temperature and OH A $^2\Sigma^+$ rotational excitation, indicating that quenching is controlled by an attractive interaction with a significant OH orientation dependence.[4–7] Several empirical models have been proposed to explain the quenching phenomena,[2,8–11] yet only recently has the mechanism for quenching of OH A $^2\Sigma^+$ by even simple molecular partners (H$_2$, N$_2$) become evident from experiment and first-principles theory.[12–24]

In order to elucidate new information about the mechanism, recent experimental studies have focused on the outcomes of collisional quenching. Two possible outcomes for quenching of OH A $^2\Sigma^+$ by H$_2$ have been examined in this laboratory: nonreactive quenching that returns OH to its ground X $^2\Pi$ electronic state,

$$\text{OH A}\,^2\Sigma^+ + \text{H}_2 \rightarrow \text{OH X}^2\Pi(v'', N'') + \text{H}_2,$$

and reactive quenching, which yields new products

$$\text{OH A}\,^2\Sigma^+ + \text{H}_2 \rightarrow \text{H} + \text{H}_2\text{O}.$$
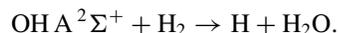
There is insufficient energy released upon quenching to access higher-energy three-body breakup channels. Previous investigations focused on the quantum state distribution of the OH X $^2\Pi$ products from nonreactive quenching under single collision conditions for several isotopic variants of this system,[13–15,21] with the most recent study focused on nonreactive quenching of OD A $^2\Sigma^+$ by H$_2$.[19] The OH/D X $^2\Pi$ products were found to exhibit extensive rotational excitation and strong Λ-doublet selectivity with minimal vibrational excitation. From product branching studies, the nonreactive pathway was shown to be a minor channel, accounting for less than 20% of quenching outcomes.[15,19] Reactive quenching was found to be the dominant channel, accounting for more than 80% of quenching events.

In this paper, we extend our recent study of the partially deuterated OD A $^2\Sigma^+$ + H$_2$ system by examining the dominant reactive quenching outcome. Previously, the translational energy release associated with reactive quenching of OH A $^2\Sigma^+$ + H$_2$ was measured by probing the H-atom products using Doppler spectroscopy on the 2s $\leftarrow\leftarrow$ 1s transition, as initially demonstrated by Anderson *et al.*[12] The Doppler profile exhibited a prominent peak near line center,

corresponding to minimal kinetic energy release, and a smaller broad component extending out to the maximum possible shift. The minimal kinetic energy release for the H-atom products implied that most of the available energy resulted in internal excitation of water, producing extremely "hot" water with internal excitation approaching its dissociation limit. Analogous studies were carried out for the OH A $^2\Sigma^+$ + D$_2$ isotopic variant,[22] with a surprising finding of both D + HOD and H + D$_2$O products. The translational energy distributions arising from reactive quenching of OH A $^2\Sigma^+$ + H$_2$/D$_2$ are revisited in the present work using an improved analysis procedure. New results are also presented for OD A $^2\Sigma^+$ + H$_2$, where again there is the possibility of distinguishing reactive quenching that occurs via H- and D-atom channels.

The D-atom products from reactive quenching of OH A $^2\Sigma^+$ by D$_2$ have also been probed using a high-n Rydberg tagging method in a crossed molecular beam experiment by Davis and co-workers.[20] A fixed-source, rotatable detector crossed molecular beams apparatus was used to determine the center-of-mass (COM) frame angular scattering of the D-atom products. The D atom products were found to be predominantly forward scattered with a minor backward component relative to incident D$_2$. The COM angular scattering distribution indicated that reactive quenching occurs primarily by a direct reaction mechanism in which the incoming OH A $^2\Sigma^+$ abstracts a D-atom from D$_2$ at relatively large impact parameters and the heavy HOD product continues in nearly the same direction as the incident OH A $^2\Sigma^+$. They also determined the kinetic energy distribution of the D-atom products, which will be compared with related experimental and theoretical results later, again showing that most of the available energy ($\sim$88%) is channeled into internal excitation of the HOD product. They were unable to examine the H-atom products due to experimental limitations.

The nonadiabatic dynamics of the OH (A $^2\Sigma^+$, X $^2\Pi$) + H$_2$ system has been the focus of numerous theoretical studies.[13,17,18,23–27] As illustrated in Figure 1, *ab initio* calculations have identified seams of conical intersection that couple the upper and lower adiabatic surfaces for configurations in which the oxygen side of the hydroxyl radical points toward the H$_2$ molecule, giving rise to barrierless pathways from OH A $^2\Sigma^+$ + H$_2$ to nonreactive OH X $^2\Pi$ + H$_2$ and reactive H + H$_2$O products, releasing 4.02 and 4.72 eV of energy, respectively.[25,26] Such calculations have been extended to map out the upper and lower adiabatic surfaces of ^{2}A$'$ symmetry as a function of OH orientation and interfragment distance, the former revealing the steep angular gradient leading toward and away from the HO-H$_2$ conical intersection region.[13] This feature of the topography has been used to explain, at least qualitatively, the high degree of rotational excitation observed for the OH X $^2\Pi$ fragments. Further insights on the nonadiabatic quenching process can be elucidated from recent classical trajectory studies of the postquenching dynamics[17,18] and nonadiabatic quantum reactive scattering calculations.[23,24] These dynamical approaches have been used to predict experimental observables, including the quantum state distributions of OH X $^2\Pi$ products, translational energy distributions of the H-atom products of reaction, and the branching ratio between nonreactive and reactive
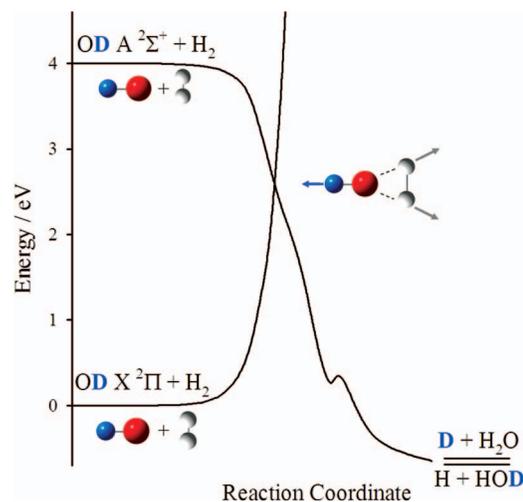

FIG. 1. Simplified reaction coordinate for quenching of OD A $^2\Sigma^+$ by H$_2$ (adapted from Ref. 27) via the C$_{2v}$ DO-H$_2$ conical intersection (from Ref. 25). Both nonreactive quenching producing OD X $^2\Pi$ + H$_2$ and reactive quenching pathways to H + HOD or D + H$_2$O products are illustrated.

pathways, as well as unobserved properties that may reflect the evolution of the system through the conical intersection region.

Han and co-workers used a time-dependent quantum wavepacket method to compute the integral cross sections for reactive and nonreactive quenching of electronically excited OH A $^2\Sigma^+$ by H$_2$ and D$_2$ as a function of collision energy based on newly developed 1A$'$ and 2A$'$ complete active space self-consistent field (CASSCF)/multi reference configuration interaction (MRCI) potentials for OH (A $^2\Sigma^+$, X $^2\Pi$) + H$_2$ in planar configurations.[23,24] In addition, they predict the vibrational and rotational state distributions of the OH X $^2\Pi$ products, the vibrational distribution of the H$_2$/D$_2$ products, and the average internal and translational energies of the products of nonreactive quenching at different collision energies. These calculations are in accord with experimental observation of highly rotationally excited OH X $^2\Pi$ products,[13–15] and predict that even greater proportions of the available energy will flow into product translation and H$_2$ vibrational excitation. They have not yet predicted the corresponding properties for the reactive quenching channel, which is the primary focus of the present experimental study.

Bowman and co-workers carried out classical trajectory calculations of the postquenching dynamics of OH A $^2\Sigma^+$ by H$_2$ and its isotopic variants,[17–19,28] starting from previously identified representative points along the seams of conical intersections.[25] The dynamical calculations were performed on a new adiabatic, full-dimensional, global potential energy surface (1A$'$) for OH X $^2\Pi$ + H$_2$ computed using the MRCI+Q/aVTZ method. They find that the branching between reactive and nonreactive quenching channels is sensitive to the initial momenta sampling method utilized, with prompt "directed" dynamics through the seams in a diabatic model predicting that reactive quenching will dominate as observed experimentally.[17,18] These authors indicate that an abstraction mechanism is strongly favored for reactive quenching, but nevertheless find evidence of a minor insertion

pathway; the latter is far more significant in experimental studies[22] as further demonstrated in the current work.

Bowman and co-workers also predict the rovibrational state distributions for the OH X $^2\Pi$ and H$_2$ products of non-reactive quenching, with high rotational and minimal vibrational excitation of OH X $^2\Pi$ products as seen experimentally. In addition, they predict high vibrational excitation of the experimentally unobserved H$_2$ products that result from the extended H–H bond in the conical intersection region. Furthermore, they compute the internal energy distribution of the H$_2$O product and the corresponding translational energy release for the reactive quenching channel, the latter of which is examined in the present work. The trajectory calculations predict that reactive quenching leads to "hot" water, which is overwhelmingly bending (ν_b) excitation with a distribution peaked at $\nu_b = 13$ ($\sim$2.5 eV). They yield a significantly smaller degree of excitation for stretches and much lower probability per quantum state with only modest rotational excitation.

This paper focuses on reactive quenching outcomes for the partially deuterated OD A $^2\Sigma^+$ + H$_2$ system. The mixed isotope system permits the H + HOD and D + H$_2$O pathways for reactive quenching to be separated from one another. Varying the isotopic composition of the system also allows a new set of observables to be measured, while keeping the electronic potential energy surfaces that control quenching unchanged. These new experimental results are compared with previous studies of OH A $^2\Sigma^+$ + H$_2$/D$_2$ reactive quenching,[12,20,22] and discussed in the context of recent theoretical studies of the quenching dynamics.

II. EXPERIMENTAL METHODS

The experimental methods are similar to those used previously in this laboratory for studies of reactive quenching of OH A $^2\Sigma^+$ by H$_2$/D$_2$.[12,22] In the present study, OD X $^2\Pi$ radicals are generated in the throat of a pulsed supersonic jet expansion by photolysis at 193 nm (Coherent COMPex 102) of DNO$_3$ (98 at. % D, 90 wt. % in D$_2$O) entrained in 30% H$_2$/He carrier gas with a backing pressure of 110 psi. In some experiments, OH X $^2\Pi$ radicals were generated in a similar fashion using HNO$_3$ (98% fuming). The UV pump laser excites the OD radicals on the A $^2\Sigma^+$ – X $^2\Pi$ (0, 0) P$_1$(1) transition at 307 nm in the collisional region of the expansion at a distance x/D = 2, where D is the nozzle diameter. The pump beam is generated by frequency doubling (KDP) the output of a Nd:YAG (532 nm) pumped dye laser (Rhodamine 640, 4–8 mJ, 7 ns, 0.08 cm^{-1}). A photomultiplier tube (PMT, ET Enterprises 9813Q) with a 308 nm bandpass filter collects the pump LIF.

After a 50 ns delay, a second spatially overlapped and counter-propagating UV probe laser beam intersects the expansion; both lasers are gently focused with 50 cm f.l. lenses. The probe beam at 243 nm is generated by frequency doubling (BBO) the output of a Nd:YAG (355 nm) pumped dye laser (Coumarin 480, 2–3 mJ, 7 ns) with an effective two-photon linewidth of 0.5 cm^{-1}. The probe laser monitors the production of H/D atoms on a two-photon (2 ^{2}S $\leftarrow\leftarrow$ 1 ^{2}S) transition. A solar blind PMT (ET Enterprises 9403B) with a

notch filter centered at 121.5 nm collects the resulting Lyman-α fluorescence.[29,30] Signals from the PMTs are preamplified, processed with a digital storage oscilloscope (LeCroy WaveRunner 6050A) and transferred to a laboratory computer for further analysis.

For the collection and integration of the H/D atom signals, an active background subtraction is utilized in order to distinguish between H/D atoms produced from the reactive quenching process and other sources of H/D atoms (background). The background subtraction scheme is implemented by operating the pump laser (5 Hz) at half the repetition rate of the probe laser (10 Hz). On alternating laser shots, the H/D atom signal arising from the probe laser only (PROBE) is subtracted from the combination of the pump and probe lasers (PUMP + PROBE), yielding the desired signal [(PUMP + PROBE) – PROBE] from reactive quenching.

There are two primary sources of background H/D atoms: photolysis of DNO$_3$ produces background D atoms (also seen in pure He as the carrier gas)[31] and reaction of OD X $^2\Pi$ with H$_2$ generates background H atoms.[32] The background H/D atoms are cooled significantly in the expansion, resulting in narrow Gaussian line profiles with typical Doppler linewidths of less than 1 cm^{-1} under these experimental conditions. The Gaussian linewidth is used to estimate the collision energy, $E_{coll} \sim 0.005$ eV, under the present experimental conditions.

Numerous tests were performed to determine the sensitivity of the H/D atom signals from quenching and background to various experimental parameters. Both signals are very sensitive to probe laser power, as expected for a two-photon transition, with a quadratic power dependence observed over the 1–3 mJ range. The H/D atom signals from quenching are unchanged with variations in photolysis laser power (40–120 mJ) and pump laser power (1–10 mJ). The H/D Doppler line shapes from quenching are unchanged over a 150 ns pump-probe time scale indicating that secondary collisions with the H$_2$/He carrier gas mixture do not change the velocity distribution of the H/D products. The best H/D signal from quenching was found at the highest backing pressure of 110 psi. These collision conditions are analogous to those used previously for detecting H/D atom products of quenching in this laboratory.[12,22]

III. RESULTS

A. Doppler profiles of H- and D-atom products

OD radicals are prepared in the lowest rovibronic level of the excited A $^2\Sigma^+$ electronic state with the pump laser and quenched by H$_2$ in the collisional region of a pulsed supersonic expansion. Typically, the OD A $^2\Sigma^+$ fluorescence lifetime is $\sim$75 ns under the present experimental conditions as determined by fitting waveform traces of the pump LIF signal to a single exponential decay. This is significantly shorter than the OD A $^2\Sigma^+$ radiative lifetime of $\sim$700 ns,[33] indicating a quenching rate of (84 ns)$^{-1}$.

The H/D atom products from reactive quenching of OD A $^2\Sigma^+$ by H$_2$ are then probed using two-photon excitation (2s $\leftarrow\leftarrow$ 1s). The Doppler profiles of the H- and D-atom products are recorded by scanning the probe laser while using active
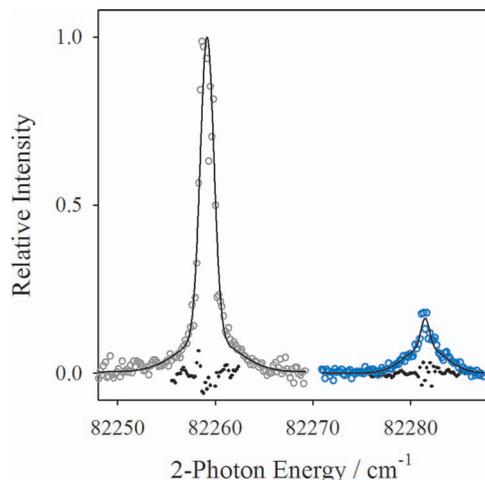
FIG. 2. Doppler profiles (○) of H (grey) and D (blue) atom products from reactive quenching of OD A $^2\Sigma^+$ by H_2, centered about their respective two-photon transitions at 82 259.2 and 82 281.5 cm^{-1}, and acquired using active background subtraction of probe laser only signals. The smooth curves through the data are added to guide the eye. Also shown are pump laser-blocked signals (●), illustrating the quality of the active background subtraction procedure near line center.

background subtraction to collect the data. The resultant Doppler profiles, summed from multiple scans to improve the signal to noise ratio, are plotted as a function of two-photon energy in Figure 2. The Doppler profiles of the H- and D-atom products are centered about their respective two-photon transitions at 82 259.2 and 82 281.5 cm^{-1}. The quality of the active background subtraction procedure used to record the data can be seen near line center with the pump laser blocked as shown by representative traces in Figure 2. The H/D signals arising from quenching [(PUMP + PROBE) – PROBE] are on the order of 7–10 times smaller than the background signals (PROBE only; not shown) at line center, yet larger than background in the wings.

The integrated areas of the Doppler profiles are proportional to the H or D product number density.[34] Therefore, the branching between the two reactive channels for quenching of OD A $^2\Sigma^+$ by H_2 can be directly determined by integrating the experimental data yielding a H:D ratio of 3:1. This shows that reactive quenching primarily forms H + HOD products that accounts for 75% of the reactive quenching outcomes. Nevertheless, the D + H_2O channel is significant, accounting for 25% of outcomes.

The H/D-atom line profiles resulting from reactive quenching of OD A $^2\Sigma^+$ + H_2 are replotted as Doppler shifts relative to line center in Figure 3. The H-atom profile is strongly peaked about line center with smaller broad contributions extending out to the maximum shift. By comparison, the D atom profile has a smaller contribution near line center, with a larger component seen in the wings spanning out to the maximum shift.

The maximum Doppler shift can be determined from the total energy available E_{avail} to the reaction products,

$$E_{avail} = E_{h\upsilon} - \Delta H_{rxn} + E_{coll},$$

where $E_{h\upsilon}$ = 4.033 eV for the OD A-X (0, 0) $P_1(1)$ transition, ΔH_{rxn} is the energy released in the ground state OD

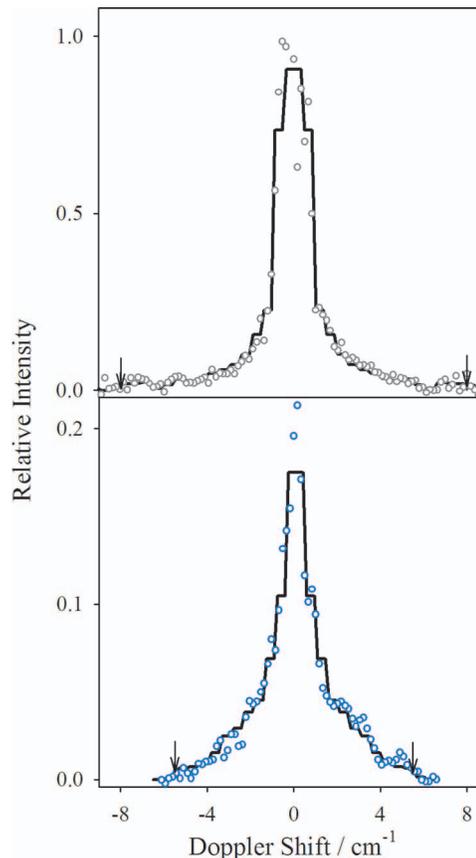FIG. 3. Doppler profiles (○) for H (grey) and D (blue) atom products arising from quenching of OD A $^2\Sigma^+$ by H_2, which is replotted from Figure 2 as Doppler shifts from line center of the respective two-photon transitions. Note the scale change in relative intensity for the lower panel. The summed discrete step functions representing the best fits to the H/D Doppler profiles (solid line) are also illustrated. The arrows indicate the maximum Doppler shifts assuming all of the available energy from reaction goes into translational energy of the H (or D) atom products.

X $^2\Pi$ + H_2 reaction (taking into account changes in enthalpy of formation for the different isotopes),[35] and E_{coll} ∼ 0.005 eV. Using conservation of energy and linear momentum, the maximum H-atom velocity is readily determined

$$v_H^{\max} = \sqrt{\frac{2E_{avail}}{m_H(1 + m_H/m_{HOD})}}.$$

From the above equations, and analogous ones for D atoms, the maximum velocities are $v_H^{\max} = 2.94 \times 10^4$ m/s and $v_D^{\max} = 2.01 \times 10^4$ m/s, corresponding to maximum Doppler shifts of ±8.06 cm^{-1} and ±5.54 cm^{-1}. The maximum Doppler shift is indicated in each panel of Figure 3 by a set of arrows.

B. Analysis of Doppler profiles

The Doppler profile is a one-dimensional projection of a three-dimensional velocity distribution along the laser propagation axis. If all of the H or D atoms were to move at the same velocity v in an isotropic spatial distribution, the Doppler profile would appear as a flat-topped box, or step function, convolved with the laser bandwidth. The experimentally observed Doppler profiles reflect a distribution of

velocities, assumed to be spatially isotropic, with varying probabilities. In order to characterize this distribution, the Doppler line shapes are fit to a series of step functions, which can be viewed as a set of discrete basis functions. The step functions have a form factor proportional to 1/v to give each box equal weighting.[36] Each basis function differs from the next by ~1800 m/s, corresponding to the 0.5 cm^{-1} effective two-photon laser linewidth. The Doppler profile is fit to the basis set in a chi-squared minimization routine by adjusting the amplitudes of the step functions using singular value decomposition. [The fitting procedure is illustrated for a simple Gaussian line profile in supplementary material.[37]] The summed discrete step functions representing the best fits to the H/D Doppler profiles are superimposed on the experimental data in Figure 3. The best fit yields a velocity probability distribution, P(v), normalized to the relative integrated areas of the H/D Doppler profiles, which can be readily converted to a product translational energy distribution, P(E$_T$).

The resultant P(E$_T$) distributions obtained from the H/D Doppler profiles recorded for reactive quenching of OD A $^2\Sigma^+$ by H$_2$ are plotted in Figure 4. Also shown are the P(E$_T$) distributions obtained by reanalyzing the H/D-atom Doppler profiles previously reported for OH A $^2\Sigma^+$ + D$_2$.[12,22] The original data and revised fit showing the summed discrete step functions are given in Figure S2 of supplementary material.[37] The H-atom Doppler profile resulting from reactive quenching OH A $^2\Sigma^+$ of H$_2$ was repeated in the present study, shown in Figure S3 of supplementary material[37] with the basis functions yielding the best fit, which gives the same P(E$_T$) distribution (Figure 4) as that derived from reanalysis of previously reported data.[12] The smooth curves through the P(E$_T$) points are a fit to the sum of two lognormal distribution functions that minimizes chi-squared, which is intended as a guide to the eye; this functional form has no inherent physical significance. Two lognormal functions were required to obtain a statistically acceptable fit for the P(E$_T$) distributions shown in top panel for OH A $^2\Sigma^+$ + H$_2$ and the D-atom channel from OD A $^2\Sigma^+$ + H$_2$ (right panel) in Figure 4. For the H-atom channel from OH A $^2\Sigma^+$ + D$_2$ (right panel), two lognormal functions give a much better fit than one, but the uncertainty at low E$_T$ limits the quality of the fit. A single lognormal distribution was adequate to obtain a good fit for the P(E$_T$) distributions shown in the left-hand panels for the mixed isotopes; only marginal improvement to the fit was obtained with the sum of two lognormal functions. (Two lognormal functions are depicted in Figure 4.)

Earlier analysis of the H/D Doppler profiles from OH A $^2\Sigma^+$ + H$_2$/D$_2$ reactive quenching was based on fitting the profiles to the sum of two Gaussian functions. The bimodal form of the Doppler profiles suggested that two different velocity distributions resulted from quenching, and each component was separately converted to a Boltzmann translational energy distribution. The present analysis makes no assumptions about the functional form of the Doppler profile, which was previously constrained to a Gaussian functional form, or resultant P(E$_T$) distribution, and thus is strongly preferred over the earlier analysis.
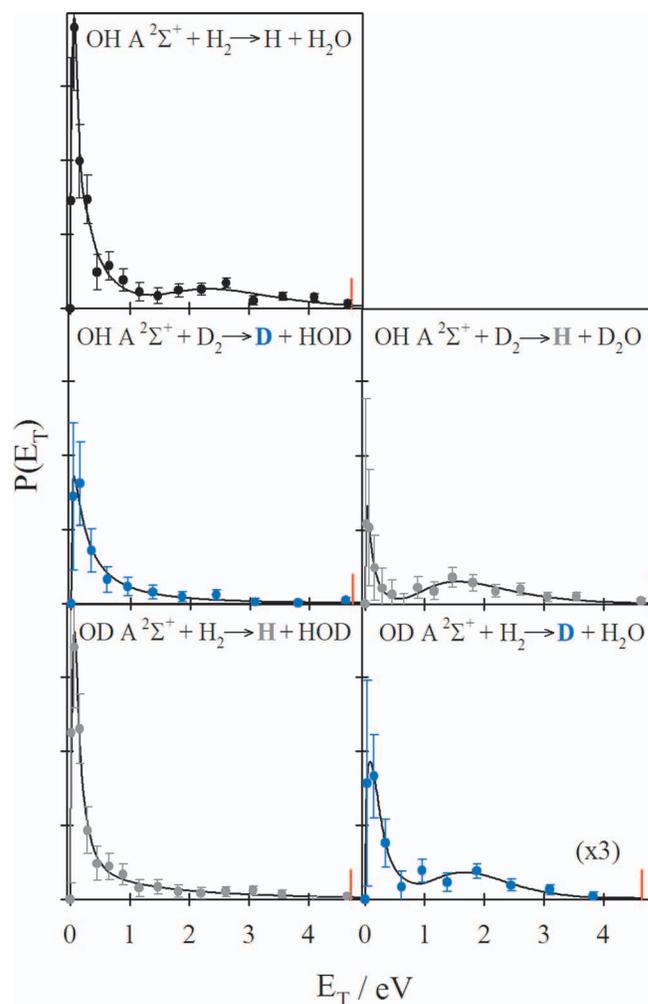

FIG. 4. Translational energy distributions, P(E$_T$), derived for the H- and D-atom products from reactive quenching of OH A $^2\Sigma^+$ + H$_2$ (top), OH A $^2\Sigma^+$ + D$_2$ (middle), and OD A $^2\Sigma^+$ + H$_2$ (bottom) with discrete points from best fits to Doppler profiles and smooth curves based on lognormal distribution functions to guide the eye. The P(E$_T$) distributions are normalized to the relative integrated areas of the H/D Doppler profiles; note the scale change for the OD A $^2\Sigma^+$ + H$_2$ → D + H$_2$O channel. Reactions yielding H- and D-atom products are color coded as grey and blue, respectively. Vertical red lines indicate available energies, which differ slightly due to changes in OH/OD transition frequency and zero-point energy for the various isotopes of water.

C. Translational energy distributions

In reactive quenching of OD A $^2\Sigma^+$ by H$_2$, the two product channels, H + HOD (75%) and D + H$_2$O (25%), exhibit distinctly different P(E$_T$) distributions (Figure 4, bottom panels). The P(E$_T$) distribution for H + HOD products exhibits a strong peak at low translational energy with approximately 2/3 of the P(E$_T$) distribution below 0.5 eV. A long tail accounts for the remaining ~1/3 of the P(E$_T$) distribution for H + HOD products, which extends to the energetic limit. The H + HOD products have an average translational energy of 0.48 eV, which corresponds to 10% of the 4.71 eV of available energy. By contrast, the pathway producing D + H$_2$O has a small peak at low translational energy (below 0.5 eV) accounting for about half of the distribution. The balance of the P(E$_T$) distribution for D + H$_2$O products lies at higher

translational energy with a distinctive secondary peak at approximately 1.8 eV and falling off toward the energetic limit. In this case, the average translational energy of the D + H_2O products is 0.82 eV, corresponding to 18% of the 4.64 eV of available energy (see Table S1).[37]

Reactive quenching of OH A $^2\Sigma^+$ by D_2 also yields different $P(E_T)$ distributions for its two channels (Figure 4, middle panels). In the primary D + HOD (60%) product channel, a peak (∼2/3) dominates the $P(E_T)$ distribution at low translational energy (below 0.5 eV). A long tail (∼1/3) stretches out to the energetic limit. In the alternate H + D_2O (40%) channel, a small peak (∼1/3) seems to be evident at low translational energy (below 0.5 eV). Most (∼2/3) of the $P(E_T)$ distribution for the H + D_2O channel is found in a broader secondary feature at higher translational energy peaking at 1.6 eV and extending to the energetic limit.

Finally, the product $P(E_T)$ distribution from reactive quenching of OH A $^2\Sigma^+$ by H_2 (Figure 4, top panel) shows a prominent peak at low translational energies (below 0.5 eV), accounting for approximately 60% of the products. This is followed by a secondary broader peak (40%) at approximately 2.6 eV with a tail that extends to the energetic limit. A discussion of the original (Gaussian) and revised fits, and the resultant $P(E_T)$ distributions for OH A $^2\Sigma^+$ + H_2/D_2 is given in supplementary material.[37]

IV. DISCUSSION

A previous study of reactive quenching in the OH A $^2\Sigma^+$ + D_2 system from this laboratory in 2001 presented a simple interpretation of the H/D translational energy distributions derived from Doppler profiles, which had been fit using the sum of two Gaussian functions that separates the $P(E_T)$ distribution into two distinct components.[22] The narrow component observed at low E_T in the D-atom channel was attributed to a direct abstraction mechanism, while the broader component seen in both D- and H-atom channels was ascribed to an insertion-like process. The broader component looked strikingly similar to a statistical distribution, although the relative intensity of the broad components in the H- and D-atom channels was not in accord with a statistical breakup (from a trigonal planar configuration). While physically intuitive, this simple picture is not adequate to explain the more comprehensive data set now available for reactive quenching that encompasses three isotopic variants: OH A $^2\Sigma^+$ + H_2, OH A $^2\Sigma^+$ + D_2, and OD A $^2\Sigma^+$ + H_2. A somewhat different picture emerges as detailed below.

We start by comparing the H/D product translational energy distributions from reactive quenching in the OD A $^2\Sigma^+$ + H_2 system with those reported previously and reanalyzed here for OH A $^2\Sigma^+$ + D_2 (Figure 4). The H- and D-atom product channels, with the departing atomic product originating from OH/D or H_2/D_2, can be separately characterized in these partially deuterated systems, but are not distinguishable from one another for the fully hydrogenated (or deuterated) system. In both systems, the dominant reactive quenching pathway is identified as the H/D products originating from H_2/D_2 with a HOD co-product, accounting for 75% of the reactive quenching products from OD A $^2\Sigma^+$ + H_2 and 60%

of the products from OH A $^2\Sigma^+$ + D_2. These H/D products have very similar translational energy distributions, as seen in the left panels of Figure 4. In both cases, the H/D products exhibit a highly peaked distribution at low translational energy (below 0.5 eV) with a long tail extending to the energetic limit. These $P(E_T)$ distributions can be represented essentially equally well by either one or the sum of two lognormal distributions, indicating that these $P(E_T)$ distributions cannot be separated into two distinct components. In addition, both release about 10% of the available energy as translation of the products.

The alternate pathways for quenching, OD A $^2\Sigma^+$ + H_2 → D + H_2O and OH A $^2\Sigma^+$ + D_2 → H + D_2O, with the H/D product originating from OH/D accounts for 25% and 40% of reactive quenching events, respectively, also give rise to $P(E_T)$ distributions that are similar to one another as shown in the right panels of Figure 4. The $P(E_T)$ distributions for these alternate pathways suggest a small peak at low translation energy (below 0.5 eV) with a distinctive secondary peak at higher translational energy (approximately 1.6–1.8 eV) in both systems. In both cases, about 20% of the available energy is deposited into product translational energy.

These alternative pathways for quenching are attributed to an insertion-like mechanism since the O from OD (or OH) appears to insert into the H_2 (or D_2) bond to form D + H_2O (or H + D_2O) products. A distinctive peak at higher E_T is seen in both cases for the insertion-like mechanism. This secondary peak is not evident in the dominant product channel, although a broad tail is observed. We are unable to determine whether or not the $P(E_T)$ distribution for the dominant product channel has a contribution from an insertion-like mechanism. We note that Davis and co-workers attributed the D-atom products detected upon quenching OH A $^2\Sigma^+$ + D_2 at higher collision energy to a direct abstraction mechanism, suggesting that the dominant product channel in the present experiments is also due to abstraction.

Adding together the $P(E_T)$ distributions for H- and D-atom products arising from OD A $^2\Sigma^+$ + H_2 or OH A $^2\Sigma^+$ + D_2 yield total $P(E_T)$ distributions which are similar to that found for the OH A $^2\Sigma^+$ + H_2 distribution (Figure 4). In OH A $^2\Sigma^+$ + H_2, there is a narrow peak at low E_T (below 0.5 eV), which is also seen for the isotopic variants studied. A higher energy secondary peak is also evident at 2.6 eV in the $P(E_T)$ distribution for OH A $^2\Sigma^+$ + H_2, which is similar to that found for the insertion-like pathways of the isotopically substituted systems. For OH A $^2\Sigma^+$ + H_2, however, the secondary peak is shifted by ∼0.8 eV to higher energy than observed for the partially deuterated variants.

For comparison, the product translational energy distributions for the OD A $^2\Sigma^+$ + H_2 system are also computed for a statistical model.[38] This model assumes complete randomization of vibrational energy in the OD–H_2 reactant pair and that the probability of forming product pairs with a particular translational energy $P(E_T)$ is proportional to the total density of states. The density of vibrational states, $N(E_v)$, is evaluated from a direct count of the HOD or H_2O product vibrational states including anharmonicity.[39] The total density of product states is then obtained by multiplying by the three-dimensional translational density of states for the

recoiling products, $E_T^{1/2}$, where $E_T + E_v = E_{avail}$, giving $P(E_T) = N(E_v)E_T^{1/2}$. The resultant statistical P(E$_T$) distributions for the H and D-atom product channels are quite similar to one another because the $E_T^{1/2}$ term dominates at higher energy where the $N(E_v)$ distributions for HOD and H$_2$O differ most significantly from one another. The statistical P(E$_T$) distributions, normalized to a peak of unity, are shown in Figure 5. (Similar results for the OH A $^2\Sigma^+$ + H$_2$/D$_2$ systems were presented in Ref. 22.) Neither the peak position (0.8 eV) nor the broad spread of the statistical P(E$_T$) distribution are in good accord with the P(E$_T$) distributions obtained from H- and D-atom Doppler profiles, indicating that reactive quenching is a nonstatistical process.[40]

Given the similarities noted above in the P(E$_T$) distributions for the systems studied by Doppler spectroscopy (Figure 4) and the limited availability of other experimental measurements and theory, we focus our comparisons on one isotopic variant, namely OH A $^2\Sigma^+$ + D$_2$. Davis and co-workers obtained the P(E$_T$) distribution shown in Figure 6 for the D + HOD products from a direct abstraction reaction based on their crossed-molecular beam scattering experiments at an average collision energy of 0.16 eV.[20] Their P(E$_T$) distribution is peaked at higher energy, 0.55 eV, and is relatively broad compared to that deduced from Doppler spectroscopy. Note that the latter experiments were carried out at a much lower collision energy of $\sim$0.005 eV in the collisional region of a supersonic expansion.

There is already abundant evidence showing that quenching of OH A $^2\Sigma^+$ by H$_2$ and other collision partners is strongly dependent on collision energy. Early kinetics studies identified a trend of decreasing cross section with increasing temperature for many molecular quenchers, which was attributed to an attractive interaction between OH A $^2\Sigma^+$ and the molecular collision partner.[2–7] More recently, Han and co-workers obtained this same trend in their nonadia-
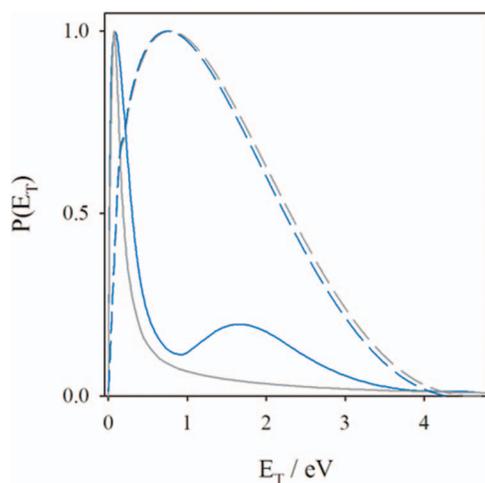

FIG. 6. Product translational energy distributions P(E$_T$) for the dominant OH A $^2\Sigma^+$ + D$_2$ $\rightarrow$ D + HOD channel. The reanalyzed P(E$_T$) distribution from Doppler profiles (blue, Ref. 22) is compared with that from crossed molecular beam experiments (red, Ref. 20). The theoretical P(E$_T$) distribution from trajectory calculations (green, Ref. 17) initiated at representative points along the seams of conical intersection is also shown. The distributions are normalized to a peak of unity.

batic quantum reactive scattering calculations for OH A $^2\Sigma^+$ + H$_2$/D$_2$.[23,24] They found reactive quenching to be the dominant process, yet the calculated integral cross section for reactive quenching decreased with increasing collision energy in the 0.06 to 0.40 eV range examined. The cross section for nonreactive quenching was essentially unchanged over this range, although one should note that the OH X $^2\Pi$ product state distribution changes, the former indicating that the branching to reactive quenching will decrease with increasing collision energy. They have not yet reported the product translational energy distribution resulting from reactive quenching or its collision energy dependence. Clearly, there is a complicated relationship between the quenching cross section, branching fraction, and the collision energy. We speculate that the change in the P(E$_T$) distributions obtained at 0.005 and 0.16 eV in experimental studies (Figure 6) may be related to the same phenomenon; alternatively, the different P(E$_T$) distributions may arise from some as yet unknown experimental source.

Bowman and co-workers have predicted P(E$_T$) distributions resulting from reactive quenching of OH A $^2\Sigma^+$ by H$_2$ and D$_2$ based on quasiclassical trajectory calculations.[17,18] The trajectories were initiated at equally weighted representative points along the seams of conical intersection, rather than the OH A $^2\Sigma^+$ + D$_2$ reactant asymptote, with an energy of 4.46 eV for zero total angular momentum. The initial momenta were sampled both fully and partially microcanonically, corresponding to models for the postquenching dynamics termed "adiabatic" and "diabatic" (with the additional constraint that $\dot{R}(0)$ is negative), with the latter in better accord with the experimental branching ratios. The resultant P(E$_T$) distribution for the D + HOD abstraction channel is reproduced in Figure 6.[17] The computed translational energy distribution peaks at 0.8 eV, which is somewhat higher in energy but similar in breadth to that observed experimentally by Davis and co-workers. Both peak at higher energy and

FIG. 5. Product translational energy distributions P(E$_T$) for OD A $^2\Sigma^+$ + H$_2$ $\rightarrow$ H (grey) + HOD and OD A $^2\Sigma^+$ + H$_2$ $\rightarrow$ D (blue) + H$_2$O channels derived from experiment represented as smooth curves based on lognormal distribution functions. Statistical distributions (dashed) are computed using the density of vibrational states for the HOD or H$_2$O products. The distributions are normalized to a peak of unity.
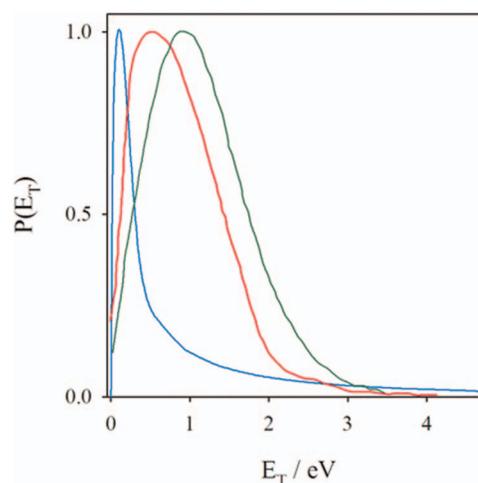
are broader than the $P(E_T)$ distribution obtained from Doppler spectroscopy. The calculated $P(E_T)$ distribution for full trajectories originating from the OH A $^2\Sigma^+$ + D$_2$ reactant asymptote and its dependence on collision energy has not yet been explored.

The predicted $P(E_T)$ distribution from trajectory calculations for the minor OH A $^2\Sigma^+$ + D$_2$ → H + D$_2$O channel (insertion) is peaked at slightly higher energy (1.2 eV) than that for the dominant channel producing D + HOD (abstraction) (see Fig. 15 of Ref. 17). In the case of OH A $^2\Sigma^+$ + H$_2$, the calculations indicate an even larger shift in the peak of the $P(E_T)$ distribution for insertion vs. abstraction (see Fig. 10 of Ref. 17). One can anticipate similar results from trajectory calculations for OD A $^2\Sigma^+$ + H$_2$. Experimentally, the secondary peak in the $P(E_T)$ distribution attributed to an insertion-like process is shifted to higher energy for OH A $^2\Sigma^+$ + H$_2$ compared to OH A $^2\Sigma^+$ + D$_2$, consistent with the trend seen in trajectory calculations. The secondary peak observed for OD A $^2\Sigma^+$ + H$_2$ is similar to that for OH A $^2\Sigma^+$ + D$_2$.

In the experimental studies, a large percentage of the reactive quenching events occur through an insertion-like process. In the quasiclassical trajectory calculations, the insertion channel accounts for only 1%–2% of the reactive quenching outcomes. The origin of this discrepancy is not known. It is interesting to note, however, that the branching ratio for the abstraction to insertion pathways differs for trajectories initiated from T-shaped HO-H$_2$ vs. linear HO–HH configurations at the CI. Specifically, C$_{2v}$ configurations yield 97.7% abstraction, while C$_{\infty v}$ configurations result overwhelmingly in abstraction (99%).[17] This suggests that insertion is more likely to occur from T-shaped HO–H$_2$ configurations than other orientations of the reactants at the CI. Furthermore, it is difficult to envision how a linear HO–HH configuration at the CI might lead directly to insertion products. Thus, we speculate that quenching dynamics originating from the OH A $^2\Sigma^+$ + H$_2$ asymptote may sample C$_{2v}$ CI configurations more heavily than suggested by equal weighting of representative points along the seams of conical intersection.

Trajectory calculations also indicate that the water products from reactive quenching of OH A $^2\Sigma^+$ by H$_2$ will be produced primarily with high bend excitation (up to v_b = 19) and a much smaller degree of asymmetric and/or symmetric stretch excitation.[17,18] Similar results were predicted for HOD produced from OH A $^2\Sigma^+$ + D$_2$.[17] Experimentally, collisional quenching of OH A $^2\Sigma^+$ by H$_2$ and its isotopic variants yield products with low translational energy on average (see Table S1).[37] This corresponds to a very high degree of internal excitation of the water products, but not sufficient energy to lead to dissociation of the water products.

A simple comparison of HO–H$_2$ configurations at representative points along the seams of conical intersections[25] with the equilibrium geometry of water provides a qualitative explanation for the high degree of internal excitation of the water products. In a direct reactive quenching process, linear C$_{\infty v}$ or near-linear configurations at the CI would lead to H-atom abstraction, but likely not insertion. Water products would emerge from the CI with highly extended H–O–H bond angles, far from the equilibrium angle, resulting in a large degree of bending excitation. Similarly, C$_{2v}$ HO–H$_2$ configurations at the CI would lead to water products from an abstraction process with extended H–O–H bond angles (159°–165°), again resulting in a large degree of bending excitation. In both of these abstraction processes, the one newly formed O–H bond (1.47–1.64 Å) is elongated at the CI compared to its equilibrium bond length, possibly leading to excitation of the asymmetric stretching mode. For HO–H$_2$ C$_{2v}$ configurations leading to insertion, the water product would emerge from the CI with a highly compressed bond angle (29°–42°), once again resulting in large bending excitation. In this case, both of the newly formed O–H bonds would be significantly longer than their equilibrium bond lengths, which could lead to symmetric stretching excitation. These simple geometric based arguments are consistent with the large internal excitation found experimentally and the large amount of bending excitation predicted in trajectory calculations.[17,18]

V. CONCLUSIONS

This paper extends the investigation of outcomes following collisional quenching of OH A $^2\Sigma^+$ + H$_2$ and its isotopic variants in this laboratory.[12–15,21,22] A recent study of nonreactive quenching for OD A $^2\Sigma^+$ + H$_2$ characterized the quantum state distribution of the OD X $^2\Pi$ (v = 0, 1) products, yielding extensive rotational excitation and a strong $\Pi(A')$ Λ-doublet selectivity, and deduced the branching fraction for OD X $^2\Pi$ products of 19.6% ± 3.6%.[19] This work focuses on the dominant reactive quenching process for OD A $^2\Sigma^+$ + H$_2$, which results in H + HOD and D + H$_2$O products with an H:D ratio of 3:1 based on the integrated areas of the Doppler profiles. Combining these results yields the following as the most significant outcomes following collisional quenching:

$$OD\,A\,^2\Sigma^+ + H_2 \rightarrow OD\,X\,^2\Pi + H_2\,(20\%)$$
$$\rightarrow H + HOD\,(60\%)$$
$$\rightarrow D + H_2O\,(20\%).$$
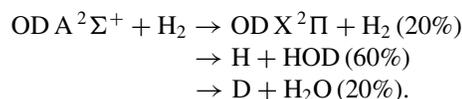
Transformation of the Doppler profiles into product translational energy distributions reveals substantial differences between the $P(E_T)$ distributions for the H- and D-atom channels. The H-atom channel is strongly peaked at low translational energy (below 0.5 eV) with a long tail extending to the energetic limit. By contrast, the D-atom channel has only a small peak at low translational energy with a relatively broad, yet distinctive secondary peak at 1.8 eV before falling off to higher energy. Reanalysis of earlier data obtained for quenching of OH A $^2\Sigma^+$ by D$_2$ shows remarkably similar product ratios and $P(E_T)$ distributions for the D + HOD and H + D$_2$O channels as those obtained for OD A $^2\Sigma^+$ + H$_2$. Further, reanalysis of Doppler profiles for quenching of OH A $^2\Sigma^+$ by H$_2$ gives a $P(E_T)$ distribution that resembles the sum of those obtained for the H- and D-atom channels, although with a clearly noticeable secondary peak at somewhat higher energy (2.6 eV) compared to the partially deuterated systems where it is ascribed to an insertion-like process. For all isotopic variants, product translation accounts for only a small amount of the available energy. The balance of the available energy is funneled into the internal excitation of the water product.

Simple geometric arguments and trajectory calculations suggest a high degree of water bend excitation.

There is now an extensive experimental data set on the reactive and nonreactive outcomes of collisional quenching for OH A $^2\Sigma^+$ + H_2 and two of its isotopic variants. Full dimensional coupled dynamics on the relevant potential energy surfaces are still needed to fully understand the nonadiabatic dynamics. Ongoing work in this laboratory is focused on exploring reactive quenching outcomes from collisions of OH A $^2\Sigma^+$ with molecular partners of importance in atmospheric and combustion environments.

ACKNOWLEDGMENTS

[1] D. R. Crosley, Adv. Ser. Phys. Chem. **3**, 256 (1995).

[2] R. A. Copeland, M. J. Dyer, and D. R. Crosley, J. Chem. Phys. **82**, 4022 (1985).

[3] D. R. Crosley, J. Phys. Chem. **93**, 6273 (1989).

[4] D. J. Creasey, D. E. Heard, M. J. Pilling, B. J. Whitaker, M. Berzins, and R. Fairlie, Appl. Phys. B **65**, 375 (1997).

[5] D. E. Heard and D. A. Henderson, Phys. Chem. Chem. Phys. **2**, 67 (2000).

[6] B. L. Hemming, D. R. Crosley, J. E. Harrington, and V. Sick, J. Chem. Phys. **115**, 3099 (2001).

[7] B. L. Hemming and D. R. Crosley, J. Phys. Chem. A **106**, 8992 (2002).

[8] P. W. Fairchild, G. P. Smith, and D. R. Crosley, J. Chem. Phys. **79**, 1795 (1983).

[9] H. M. Lin, M. Seaver, K. Y. Tang, A. E. W. Knight, and C. S. Parmenter, J. Chem. Phys. **70**, 5442 (1979).

[10] P. H. Paul, J. Quant. Spectrosc. Radiat. Transf. **51**, 511 (1994).

[11] A. E. Bailey, D. E. Heard, D. A. Henderson, and P. H. Paul, Chem. Phys. Lett. **302**, 132 (1999).

[12] D. T. Anderson, M. W. Todd, and M. I. Lester, J. Chem. Phys. **110**, 11117 (1999).

[13] P. A. Cleary, L. P. Dempsey, C. Murray, M. I. Lester, J. Kłos, and M. H. Alexander, J. Chem. Phys. **126**, 204316 (2007).

[14] L. P. Dempsey, C. Murray, P. A. Cleary, and M. I. Lester, Phys. Chem. Chem. Phys. **10**, 1424 (2008).

[15] L. P. Dempsey, C. Murray, and M. I. Lester, J. Chem. Phys. **127**, 151101 (2007).

[16] L. P. Dempsey, T. D. Sechler, C. Murray, M. I. Lester, and S. Matsika, J. Chem. Phys. **130**, 104307 (2009).

[17] B. Fu, E. Kamarchik, and J. M. Bowman, J. Chem. Phys. **133**, 164306 (2010).

[18] E. Kamarchik, B. N. Fu, and J. M. Bowman, J. Chem. Phys. **132**, 091102 (2010).

[19] J. H. Lehman, L. P. Dempsey, M. I. Lester, B. Fu, E. Kamarchik, and J. M. Bowman, J. Chem. Phys. **133**, 164307 (2010).

[20] M. Ortiz-Suárez, M. F. Witinski, and H. F. Davis, J. Chem. Phys. **124**, 201106 (2006).

[21] I. B. Pollack, Y. X. Lei, T. A. Stephenson, and M. I. Lester, Chem. Phys. Lett. **421**, 324 (2006).

[22] M. W. Todd, D. T. Anderson, and M. I. Lester, J. Phys. Chem. A **105**, 10031 (2001).

[23] P. Y. Zhang, R. F. Lu, T. S. Chu, and K. L. Han, J. Chem. Phys. **133**, 174316 (2010).

[24] P. Y. Zhang, R. F. Lu, T. S. Chu, and K. L. Han, J. Phys. Chem. A **114**, 6565 (2010).

[25] B. C. Hoffman and D. R. Yarkony, J. Chem. Phys. **113**, 10091 (2000).

[26] D. R. Yarkony, J. Chem. Phys. **111**, 6661 (1999).

[27] M. I. Lester, R. A. Loomis, R. L. Schwartz, and S. P. Walch, J. Phys. Chem. A **101**, 9195 (1997).

[28] J. M. Bowman, G. Czako, and B. Fu, Phys. Chem. Chem. Phys. **13**, 8094 (2011).

[29] C. L. Cesar, D. G. Fried, T. C. Killian, A. D. Polcyn, J. C. Sandberg, I. A. Yu, T. J. Greytak, D. Kleppner, and J. M. Doyle, Phys. Rev. Lett. **77**, 255 (1996).

[30] T. W. Hansch, S. A. Lee, R. Wallenstein, and C. Wieman, Phys. Rev. Lett. **34**, 307 (1975).

[31] A. A. Turnipseed, G. L. Vaghjiani, J. E. Thompson, and A. R. Ravishankara, J. Chem. Phys. **96**, 5887 (1992).

[32] M. Alagia, N. Balucani, P. Casavecchia, D. Stranges, G. G. Volpi, D. C. Clary, A. Kliesch, and H. J. Werner, Chem. Phys. **207**, 389 (1996).

[33] J. Luque and D. R. Crosley, SRI International Report No. MP 99–009, 1999.

[34] G. W. Johnston, H. Kornweitz, I. Schechter, A. Persky, B. Katz, R. Bersohn, and R. D. Levine, J. Chem. Phys. **94**, 2749 (1991).

[35] M. W. Chase, J. L. Curnutt, J. R. Downey, R. A. McDonald, A. N. Syverud, and E. A. Valenzuela, J. Phys. Chem. Ref. Data **11**, 695 (1982).

[36] R. N. Zare and D. R. Herschbach, Proc. IEEE **51**, 173 (1963).

[37] See supplementary material at http://dx.doi.org/10.1063/1.3644763 for additional information on the analysis procedure and a table compiling experimental and theoretical results.

[38] M. N. R. Ashfold, R. N. Dixon, M. Kono, D. H. Mordaunt, and C. L. Reed, Philos. Trans. R. Soc. London, Ser. A. **355**, 1659 (1997).

[39] N. Gailar and E. K. Plyler, J. Chem. Phys. **24**, 1139 (1956).

[40] This differs from the prior analysis for OH A $^2\Sigma^+$ + D_2, where the broad components of the H/D P(E_T) distributions were interpreted as being similar to statistical distributions. See also Ref. 22.